Journal of ELECTRONIC MATERIALS, Vol. 47, No. 7, 2018
https://doi.org/10.1007/s11664-018-6295-5

Room Temperature Gas Sensing Properties of Sn-Substituted Nickel Ferrite ($NiFe_2O_4$) Thin Film Sensors Prepared by Chemical Co-Precipitation Method

V. MANIKANDAN,[1,5] XIAOGAN LI,[2] R.S. MANE,[3] and J. CHANDRASEKARAN[4]

1.—Department of Physics, RVS Technical Campus, Coimbatore, Tamil Nadu 641402, India. 2.—School of Electronic Science and Technology, Dalian University of Technology, Dalian 116023, People's Republic of China. 3.—Center for Nanomaterial and Energy Devices, Swami Ramanand Teerth Marathwada University, Dnyanteerth, Vishnupuri, Nanded 431606, India. 4.—Department of Physics, Sri Ramakrishna Mission Vidyalaya College of Arts and Science, Coimbatore, Tamil Nadu 641 020, India. 5.—e-mail: manikandan570@gmail.com

Tin (Sn) substituted nickel ferrite ($NiFe_2O_4$) thin film sensors were prepared by a simple chemical co-precipitation method, which initially characterized their structure and surface morphology with the help of x-ray diffraction and scanning electron microscopy. Surface morphology of the sensing films reveals particles stick together with nearer particles and this formation leads to a large specific area as a large specific area is very useful for easy adsorption of gas molecules. Transmission electron microscopy and selected area electron diffraction pattern images confirm particle size and nanocrystallnity as due to formation of circular rings. Fourier transform infrared analysis has supported the presence of functional groups. The 3.69 eV optical band gap of the film was found which enabled better gas sensing. Gas sensors demonstrate better response and recovery characteristics, and the maximum response was 68.43%.

Key words: Nanostructured ferrites, gas sensor, thin film, surface morphology

INTRODUCTION

In recent decades, sulfur hexafluoride has been used in gas insulated switch gears mainly in power electronics owing to its outstanding features like small floor space, stability, reliability, insulation and low cost. It is denser than air because of its robust capture of oxygen and has a good dielectric strength. Due to sufficient dielectric strength, it is used as an insulating medium. So, it is inevitable in gas insulated switch gears.[1–3] The pure sulfur hexafluoride is nontoxic, colorless and non-flammable. During the filling of the target gas at pressure, it can be leaked. The leaked gases can be easily mixed with oxygen, leading to increased toxicity. The above mixtures of gas release toxic gases like sulfur dioxide and hydrogen fluoride. Hence, sulfur hexafluoride is essential for electrical equipment and environmental safety.[4–6] To date, numerous methods have been used to detect sulfur hexafluoride, and the methods are namely gas chromatography, semiconductor gas detection tubes and infrared absorption spectrometry. Decomposed low-level fluorine sulfides cannot be detected through gas detection tubes. In gas chromatography, it takes more time for detection and also offline testing is irremissible.[7,8] Mostly, thin film types of gas sensors are used in detection. However, a thin film gas sensor detects oxidizing and reducing gas and a thick film detects only reducing gases.[9] Specifically, transition-metal oxides with d0 and d10 electronic configurations are being used for gas sensor applications.[10] The d10 electronic configuration is shown in the post-transition-metal oxide of tin (Sn). Due to this reason, tin (Sn) elements can be substituted in nickel ferrite film.

(Received December 17, 2017; accepted April 10, 2018; published online April 25, 2018)

Moreover, the detection of the sulfur hexafluoride gas using tin (Sn) substituted nickel ferrite sensor is seldom reported. Currently, ferrite based gas sensors are being used for detecting toxic gases because of their simple fabrication process, abundancy, chemical and environmental stability, reliability and low cost.[11,12] The selectivity of the sensor refers to characteristics of the sensor material. To be precise, the ternary compounds have high chemical stability and, thereby, huge potential in gas sensor applications.[13,14] Nickel ferrite is an inverse spinel wherein the nickel ions occupy the octahedral sites. Substituting metal cations on nickel ferrites has developed new structures for delivering better gas sensing performance as conduction in spinel ferrites occurs via electron or hole transfer among equal cations located in the octahedral sites, sensitive to chemical composition.[15] Normally, nickel ferrites have high electrical resistances which on substituting Sn can be decreased, that is beneficial for the gas sensing process. In this work, we report an easy and effective chemical co-precipitation method to prepare sensor material. Particularly, the analysis is mainly focused on the sensing behavior of Sn-$NiFe_2O_4$ against sulfur hexafluoride gas. The fabricated sensor material exhibits good response to sulfur hexafluoride gas. Also, active sites are easily interacting with oxygen molecules when compared to other ferrite materials.

In addition to this, the fabricated sensor is a novel material used for a room temperature (27°C) sulfur hexafluoride gas sensing application which is eco-friendly and economically cheap.[16–21] Table I shows a short literature evaluation of some materials as sensors in past years.

EXPERIMENTAL DETAILS

Synthesis of Sn-$NiFe_2O_4$

Tin chloride, nickel chloride and ferric chloride were used as starting materials and these materials were dissolved in de-ionized water which was kept with vigorous stirring for 2 (h) and then sodium hydroxide solution was added drop by drop until pH 11. After pH 11, the mixture solution was changed to dark brown. The brown precipitate was scrupulously washed with the help of de-ionized water to remove the chlorine and other impurities, if there was any. Then, the powders were dried at overnight in a hot air oven and finally, the dried powders were put into a mortar and ground manually for 1 (h) for their fineness. The prepared material is $x = 0.2$ concentration ($Sn_xNi_{1-x}Fe_2O_4 = Sn_{0.2}Ni_{0.8}Fe_2O_4$).

Fabrication of Film Sensors

The thin film sensors were obtained on borosilicate substrates by using the spin coating technique. The substrate has the dimension of 1.5 × 1.5 cm^2. The substrate was washed in an ultrasonic cleaner by immersion in de-ionized water followed by iso propyl alcohol and then acetone for 15 (min). Next, the substrate was dried in a hot air oven at 150°C for 10 (min). One layered Sn-$NiFe_2O_4$ thin film sensor was obtained on the substrate by using a photo resist spinner at a speed of 3000 rpm and then dried at 70°C on a hot plate. Likewise, a number of layers was deposited. The distribution of nanoparticles is uniform on the substrate. The thickness of the sensor was 16 μm. The prepared thin films were sintered at 900°C for 4 (h) in a muffle furnace and were used for structure, morphology and gas sensor measurements.

RESULTS AND DISCUSSION

Structural Elucidation

Figure 1 shows the x-ray diffraction (XRD) pattern of the Sn-$NiFe_2O_4$ film sensor. The diffraction

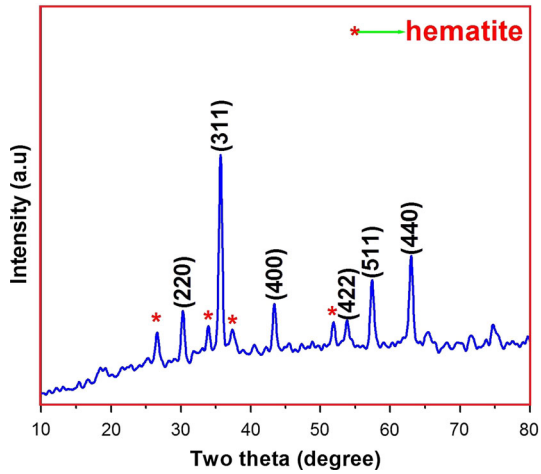

Fig. 1. XRD pattern of Sn substituted nickel ferrite film.

Table I. Comparison of sensing results of earlier reported sensing materials

Materials	Target gas	Optimum temperature	% sensor response	References
SnO_2/MWCNTs	SF_6	90°C	36.5	34
Zno nanorods	SF_6	420°C	18.06	35
Au doped TiO_2	SF_6	110°C	42.3	36
Pt doped TiO_2	SF_6	200°C	24.07	37
Sn doped $NiFe_2O_4$	SF_6	25°C	68.43	–

angles at $2\theta = 30.27$, 35.67, 43.34, 53.84, 57.35, 62.92 are assigned to (220), (311), (400), (422), (511) and (440) reflection planes. All diffraction peaks are in accordance with the values found in the standard card (JCPDS-74-2081) and can be indexed as typical cubic structure. The relatively high intensity (311) peak confirms the formation of Sn-$NiFe_2O_4$. Also, the hematite phase is observed in Sn-$NiFe_2O_4$. It is due to the loss of divalent elements in the prepared material. The estimated average crystallite size is in the range of 39 nm found by using the Debye–Scherrer formula.[22]

Surface Morphology Analysis

The surface morphology of the sensing film was confirmed through scanning electron microscopy. Figure 2a shows spherical nanoparticles with porous architecture. In addition to these, particles are of non-uniform sizes and well agglomerated. From surface morphology results, sensing films have large specific areas, and they are very useful for adsorption processes. Also, the high surface of the film consists of highly reactive dangling bonds, which are highly appreciated in gas sensor applications.[23] Owing to this, the film was ready for adsorption of the gas. Figure 2b shows an energy dispersive x-ray (EDX) spectrum that reveals Ni, O, Sn, and Fe elements of Sn-$NiFe_2O_4$ (Chemical composition—$Sn_{0.2}Ni_{0.8}Fe_2O_4$).

FT-IR Spectroscopy Analysis

Figure 3 shows the FT-IR spectrum of the Sn-$NiFe_2O_4$ film sensor. The Sn-$NiFe_2O_4$ film shows strong peaks at 3419 cm^{-1}, 2978 cm^{-1}, and 2372 cm^{-1} respectively. The strong and high intensity peak at 3419 cm^{-1} is due to the presence of stretching and bending of H–O–H vibrations.[24] The peak at 2978 cm^{-1} indicates the presence of hydrogen bonding.[25] The peak at 2372 cm^{-1} is owing to a C = O stretch which is attributed to atmospheric[26] CO_2. In addition to these strong peaks, there is a low intensity peak observed at 598 cm^{-1} which corresponds to the usual behavior of ferrites.[27] The strong peak is owing to the water adsorbed from air as due to porous Sn-$NiFe_2O_4$ is also seen.[28] Hence, sintering is required to complete the solid state reaction and also eliminate impurities or other unwanted elements there.

TEM Analysis

The microstructure, particle size and structure type of Sn-$NiFe_2O_4$ nanoparticles were investigated through transmission electron microscopy (TEM). Figure 4a shows at 35.02, 46.03 and 34.51 nm the particle sizes of Sn-$NiFe_2O_4$. Thus, particles were non-uniform in sizes and inhomogeneous formation.

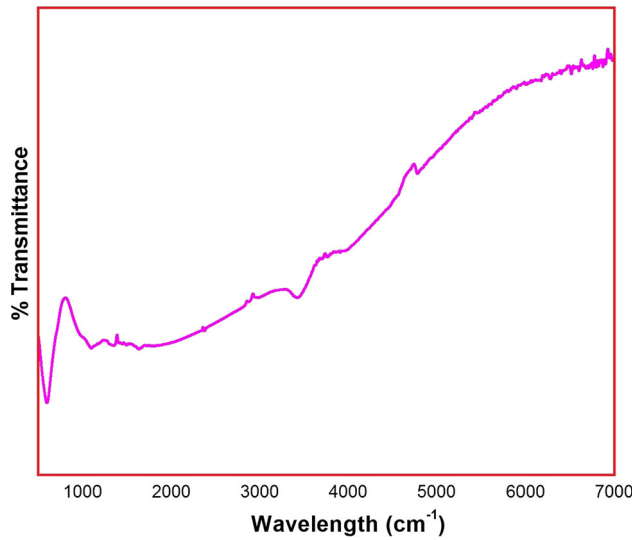

Fig. 3. FTIR spectrum of Sn substituted nickel ferrite film.

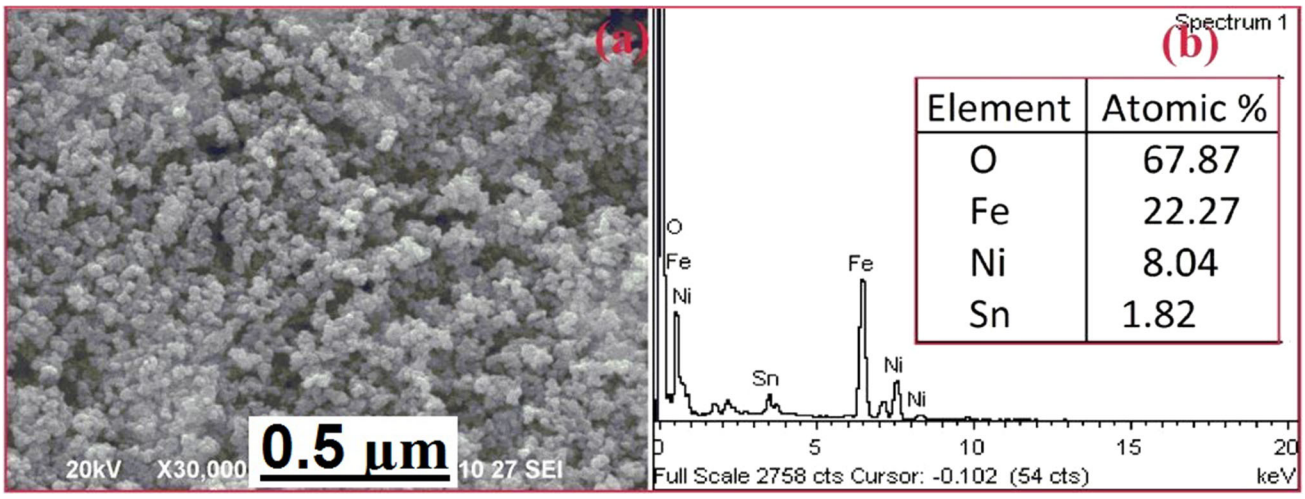

Fig. 2. (a) Surface morphology and (b) EDX spectrum Sn substituted nickel ferrite film.

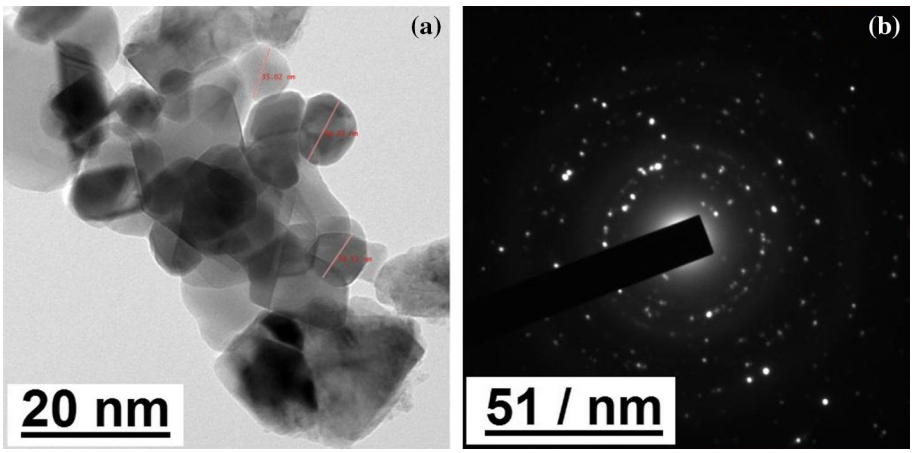

Fig. 4. (a) TEM microstructure and (b) SAED pattern of Sn substituted nickel ferrite film.

Also, Sn-$NiFe_2O_4$ nanoparticles have spherical structure. Besides, Fig. 4b shows the circular rings and SAED pattern designating the nanocrystalline signature of Sn-$NiFe_2O_4$.[29,30]

UV–Vis Absorption Spectroscopy

The optical absorption spectrum of a Sn-$NiFe_2O_4$ sensor and Tauc's plot is shown in Fig. 5a and b. It is found that the material has absorption in the visible region at ~ 233.31 nm. The variation of the optical absorption coefficient (α) and its corresponding variation in photon energy (eV) are calibrated from the absorbance and wavelength. The optical band gal energy (E_g) of a Sn-$NiFe_2O_4$ sensor can be calibrated from the following relation;

$$E_g = h\vartheta - (\alpha h\vartheta)^{1/n}, \quad (1)$$

where ϑ is the transition frequency, and the exponent 'n' characterizes the nature of the band transition and the transition of the direct allowed type, therefore n = 1/2 (n = 1/2 and 3/2 correspond to direct allowed and direct forbidden transition when n = 2 and 3 correspond to indirect allowed and indirect forbidden transition). The optical band gap energy (E_g) is calibrated by extrapolating the curve to zero absorption. The calibrated band gap of the sensing film was found to be 3.69 eV.

Sensing Properties

In a gas chamber, sulfur hexafluoride was loaded in two different volumes and variations in time and resistance were recorded by a Keithley Electrometer 6514. Figure 6 depicts the response of the gas sensor with different volumes in ppm. Firstly, the resistance of the sensor increases to a stable value when the injection of gas in the gas chamber is done. This value can be taken as resistance in air (R_a). Then, the resistance value decreases owing to elimination of gas from the gas chamber. This value can be taken as resistance in the gas-air mixture (R_g). With 80 ppm concentration (gas), the resistance of the sensor is increased, and it shows a sensing curve. With increase of concentration (gas), again the resistance value is increased with better sensing and repeatability signatures as compared to the first one. The repeatability designates the suitability of the sensor material as a sulfur hexafluoride gas sensor. From the sensing curve results, increase of sensitivity and percentage of sensor response were increased due to the rise of gas concentration, this achieves 0.59 Sensitivity which was calculated from the sensing curve and using the following reaction;

$$\text{Sensitivity} = R_g/R_a. \quad (2)$$

The percentage of the sensor is defined as;

$$\text{Percentage of sensor response} = \frac{|R_a - R_g|}{R_a} * 100. \quad (3)$$

The maximum sensor response is ~ 68.43%. Then, response and recovery time figures of the Sn-$NiFe_2O_4$ sensor are important parameters in sensor applications. The response time is defined as time taken by the film to attain 90% of the resistance. The time taken by the film to reduce the 90% resistance value is nothing but recovery time. A Sn-$NiFe_2O_4$ gas sensor demonstrates better response and recovery signatures, i.e., 3.76 and 23.21 (min) for 68% of its full response and recovery. From the sensing curve results, the pure nickel ferrite shows less sensitivity as compared to Sn-$NiFe_2O_4$. The Sn-$NiFe_2O_4$ sensor reveals an enhanced sensitivity for the sulfur hexafluoride gas. This may be due to the partial replacement of nickel ions by tin ions at octahedral sites which is of advantage for the adsorption process[31] and d10 electronic configuration.[10] This is also one of the factors that increases the sensitivity of Sn-$NiFe_2O_4$. The sensing mechanism can be explained on the basis of adsorption of

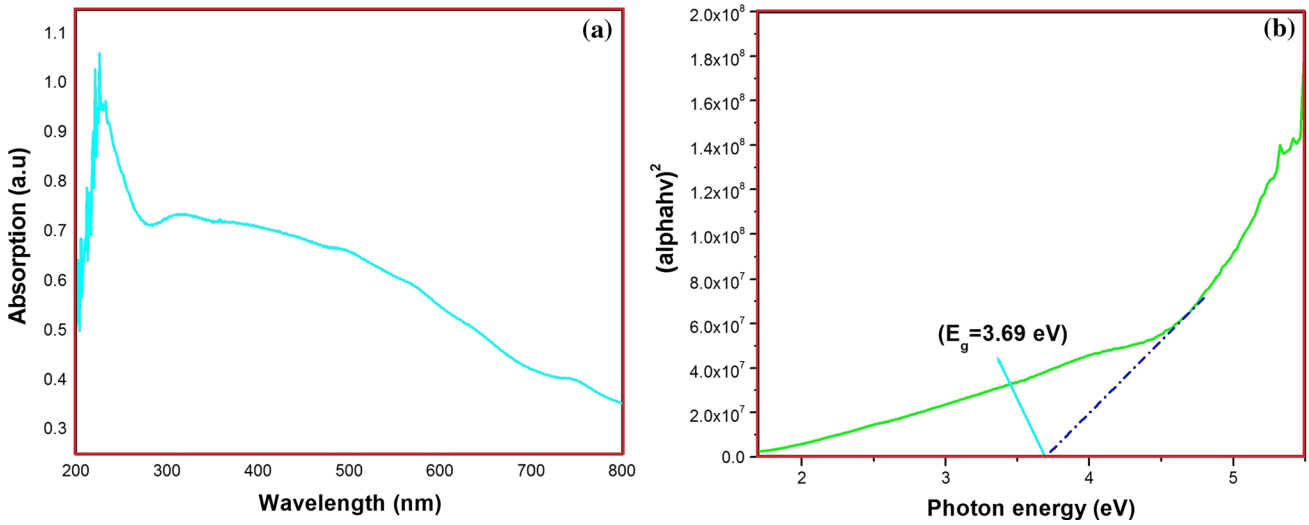

Fig. 5. (a) Absorption spectra and (b) Tauc's plot for Sn substituted nickel ferrite film.

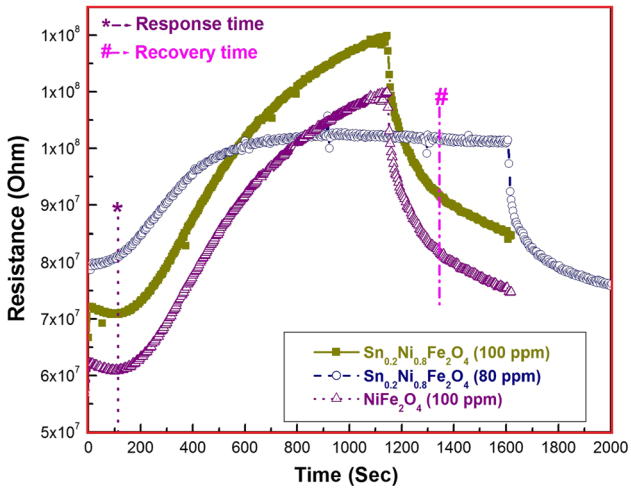

Fig. 6. Gas sensing behavior of Sn substituted nickel ferrite film.

oxygen molecules.[32] In an air atmosphere, oxygen molecules ionize into O^-_{ads} or O^{2-}_{ads} by capturing the free electron from the nanoparticles. Due to this action, the conductivity reduces and also resistance increases. On exposing of sulfur hexafluoride gas on sensing film, the gas molecules may adsorb. With the effect of adsorption, the gas molecules act as electron acceptors and, thereby, the resistance of the Sn-$NiFe_2O_4$ film sensor increases. The following chemical reactions may take place on the surface of the Sn-$NiFe_2O_4$ film sensor;[33]

$$O_2 + e^- \leftrightarrow O^-_{ads}, \quad (4)$$

$$SF_{6(gas)} + e^- \rightarrow SF^-_{6(ads)}. \quad (5)$$

The above reactions indicate that decrease of the number of electrons followed an increase of Sn-$NiFe_2O_4$ film sensor resistance.[33] Additionally, the following reaction occurred between SF^-_{6ads} and O^-_{ads};

$$SF^-_{6\,ads} + O^-_{ads} \rightarrow 2O^{2-}_{ads} + SF_6. \quad (6)$$

From the gas sensor analysis, the prepared Sn-$NiFe_2O_4$ film sensor finds its suitability as a room temperature sulfur hexafluoride gas sensor.

CONCLUSION

A simple and cost effective method has been used to fabricate the Sn-$NiFe_2O_4$ film sensor. X-ray diffraction (XRD) analysis confirms the presence of cubic structure and also formation of ferrite. The surface morphology shows the porous surface with the spherical structure of nanoparticles. Transmission electron microscopy (TEM) microstructure reveals the particle size and crystalline nature of materials. In Fourier transform infrared (FTIR) analysis, low intensity peaks show the usual behavior of ferrites. The 3.69 eV optical band gap was achieved and the wide optical band gap enables the good sensing behavior of the film. The prepared Sn-$NiFe_2O_4$ film sensor exhibits excellent response and recovery signatures for sulfur hexafluoride gas. From the gas sensor measurements, the Sn-$NiFe_2O_4$ film sensor shows 68.43% maximum response.

CONFLICT OF INTEREST

The authors declare that they have no conflict of interest.

REFERENCES

1. M. Kawamura, K. Ishi, and S. Sato, *J. Appl. Phys.* 36, 4517 (1997).
2. A. Derdouri, J. Casanovas, R. Hergli, R. Grob, and J. Mathieu, *J. Appl. Phys.* 65, 1852 (1989).
3. H. Dai, P. Xiao, and Q. Lou, *Phys. Status Solidi Appl. Mater. Sci.* 208, 1714 (2011).

4. F. Deng, Y. He, G. Shi, B. Li, and X. Wu, *Sens. Actuators B Chem.* 237, 120 (2016).
5. L. Tang, Y. Li, K. Xu, X. Hou, and Y. Lv, *Sens. Actuators B Chem.* 132, 243 (2008).
6. Y. Wu, S. Zhang, X. Wang, N. Na, and Z. Zhang, *Luminescence* 23, 376 (2008).
7. R. Kurte, C. Beyer, H.M. Heise, and D. Klockow, *Anal. Bioanal. Chem.* 373, 639 (2002).
8. J.M. Braun and F.Y. Chu, *IEE. Trans. Power. Syst.* 2, 81 (1986).
9. G. Mu, *Sens. Actuators B Chem.* 77, 55 (2001).
10. X. Liu, S. Cheng, H. Liu, S. Hu, D. Zhang, and H. Ning, *Sensors* 12, 9635 (2012).
11. M. Singh, B.C. Yadav, A. Ranjan, R.K. Sonker, and M. Kaur, *Sens. Actuators B Chem.* 249, 96 (2017).
12. A. Singh, A. Singh, S. Singh, P. Tandon, B.C. Yadav, and R.R. Yadav, *J. Alloys Compd.* 618, 475 (2015).
13. P. Reñones, M.C. Alvarez-Galvan, L. Ruiz-Matas, M. Retuerto, R.M. Navarro, and J.L.G. Fierro, *Mater. Today Energy* 6, 248 (2017).
14. F. Falsafi, B. Hashemi, A. Mirzaei, E. Fazio, F. Neri, N. Donato, S.G. Leonardi, and G. Neri, *Ceram. Int.* 43, 1029 (2017).
15. A. Sutka, G. Mezinskis, A. Lusis, and M. Stingaciu, *Sens. Actuators B Chem.* 171, 354 (2012).
16. S. Pandey, B. Kyun, S. Ryul, D. Hyeon, and D. Ho, *J. Sci. Adv. Mater. Dev.* 2, 263 (2017).
17. R. Dhahri, M. Hjiri, L. El Mir, H. Alamri, A. Bonavita, D. Iannazzo, S.G. Leonardi, and G. Neri, *J. Sci. Adv. Mater. Dev.* 2, 34 (2017).
18. M.H. Suhail, A.A. Ramadan, S.B. Aziz, and O.G. Abdullah, *J. Sci. Adv. Mater. Dev.* 2, 301 (2017).
19. V.-M. Rodríguez-Betancourtt, H.G. Bonilla, M.Flores Martínez, A. Guillén Bonilla, J.P. Moran Lazaro, J.T.G. Bonilla, M.A. González, M. De La Luz Olvera Amador, *J. Nanomater.* (2017). https://doi.org/10.1155/2017/8792567.
20. M.A. Basyooni, M. Shaban, and A.M. El Sayed, *Sci. Rep.* 7, 1 (2017).
21. D.D. Trung, N.D. Cuong, K.Q. Trung, T.D. Nguyen, N. Van Toan, C.M. Hung, and N. Van Hieu, *J. Alloys Compd.* 735, 787 (2018).
22. V. Manikandan, A. Vanitha, E.R. Kumar, and S. Kavita, *J. Magn. Magn. Mater.* 426, 11 (2017).
23. B.C. Yadav, S. Singh, and A. Yadav, *Appl. Surf. Sci.* 257, 1960 (2011).
24. R.K. Swarnkar, S.C. Singh, and R. Gopal, *Bull. Mater. Sci.* 34, 1363 (2012).
25. C. Meiorin, D. Muraca, K.R. Pirota, M.I. Aranguren, and M.A. Mosiewicki, *Eur. Polym. J.* 53, 90 (2014).
26. N. Shukla, C. Liu, P.M. Jones, and D. Weller, *J. Magn. Magn. Mater.* 266, 178 (2003).
27. V. Manikandan, A. Vanitha, E. Ranjith Kumar, and J. Chandrasekaran, *J. Magn. Magn. Mater.* 423, 250 (2017).
28. B.C. Yadav, K.S. Chauhan, S. Singh, R.K. Sonker, S. Sikarwar, and R. Kumar, *J. Mater. Sci.: Mater. Electron.* 28, 5270 (2017).
29. V. Manikandan, N. Priyadharsini, S. Kavita, and J. Chandrasekaran, *Superlattices Microstruct.* 109, 648 (2017).
30. V. Manikandan, A. Vanitha, E. Ranjith Kumar, and J. Chandrasekaran, *J. Magn. Magn. Mater.* 432, 477 (2017).
31. A.V. Kadu, S.V. Jagtap, and G.N. Chaudhari, *Curr. Appl. Phys.* 9, 1246 (2009).
32. S. Singh, B.C. Yadav, V.D. Gupta, and P.K. Dwivedi, *Mater. Res. Bull.* 47, 3538 (2012).
33. I. Madhi, B. Bouzid, M. Saadoun, and B. Bessaïs, *Ceram. Int.* 41, 6552 (2015).
34. H.F. Dai, P. Xiao, and Q. Lou, *Phys. Status Solidi A* 7, 1714 (2011).
35. S. Peng, G. Wu, W. Song, Q. Wang, J. Nanomaterials, Article ID 135147 (2013).
36. X. Zhang, Y. Lei, J. Tie, and X. Dong, *Sensors* 14, 19517–19532 (2014).
37. X. Zhang, J. Tie, and J. Zhang, *Sensors* 13, 14764–14776 (2013).